Hydrogen-enhanced fatigue crack growth behaviors in a ferritic Fe-3wt%Si steel studied by fractography and dislocation structure analysis

Di Wan[a,*], Antonio Alvaro[b], Vigdis Olden[b], Afrooz Barnoush[a]

a. Department of Mechanical and Industrial Engineering, Norwegian University of Science and Technology, Richard Birkelands vei 2B, 7491 Trondheim, Norway

b. SINTEF Industry, 7456 Trondheim, Norway

Email: di.wan@ntnu.no

*Corresponding author

Abstract

The effect of hydrogen (H) on the fatigue behavior is of significant importance for metallic structures. In this study, the hydrogen-enhanced fatigue crack growth rate (FCGR) tests on in-situ electrochemically H-charged ferritic Fe-3wt%Si steel with coarse grain size were conducted. Results showed strong difference between the H-charged and the non-charged conditions (reference test in laboratory air) and were in good agreement with the results from literature. With H-charging, the fracture morphology changed from transgranular (TG) type to "quasi-cleavage" ("QC"), with a different fraction depending on the loading frequency. With the help of electron channeling contrast imaging (ECCI) inside a scanning electron microscope (SEM), a relatively large area in the failed bulk specimen could be easily observed with high-resolution down to dislocation level. In this work, the dislocation sub-structure immediately under the fracture surfaces were investigated by ECCI to depict the difference in the plasticity evolution during fatigue crack growth (FCG). Based on the analysis, the H-enhanced FCG mechanisms were discussed.

Keywords: hydrogen embrittlement; fractography; Fe-3wt%Si; fatigue crack growth (FCG); SEM; ECCI.

1. Introduction

The hydrogen embrittlement (HE) effect of metallic materials has been intensively studied through the last decades. Several mechanisms have been developed based on the interaction between hydrogen and metals[1] among which hydrogen-enhanced localized plasticity (HELP) [2-7], hydrogen-enhanced decohesion (HEDE) [8-11] and adsorption-induced dislocation-emission (AIDE) [12] gained the most credibility among the scientific community. The HELP mechanism considers the hydrogen (H) effect on promoting the dislocation motion and generation and thus localized plastic zone and increase in the local stress state, which leads to an early fracture. In the HEDE mechanism H acts towards weakening the interatomic bonds in the material therefore promoting brittle fracture. The AIDE mechanism involves the weakening of interatomic bonding at the crack tips due to adsorbed H, which leads to cleavage-like and intergranular fractures. In practice, there could be several mechanisms simultaneously affecting

the fracture behavior of the metallic structures [13] and hence, special attention should be paid when considering different cases.

Metal fatigue is one of the main reasons behind catastrophic failures of modern engineering structures, costing a large amount of economical loss and sometimes even fatality each year [14]. The presence of H in the material can enhance the metallic component's fatigue crack growth rate (FCGR) leading to even earlier dangerous unexpected failures. In other words, the presence of H can ruin the primary fatigue design and life estimation of the structures in service. Oil platforms, for example, experience continuously oscillatory environmental loads with the presence of H. Degradation by H under such conditions would obviously lead to a reduction of the fatigue life of the structures. Hence, it is a critical issue to investigate and analyze the fatigue failure under H environments, which can help to improve the understanding of the mechanical behaviors and improve the fatigue design.

Classically, the fatigue crack growth (FCG) behavior of materials is characterized by three stages, namely crack initiation and slow growth (stage I), stable crack propagation (stage II) and a strongly accelerated crack growth rate which lead to unstable sudden fracture (stage III). Among these three regions, the stage II FCG behavior is usually described by the Paris' (also known as Paris-Erdogan) law as a mathematical relation, of which the basic equation reads as Eq. 1:

$$\frac{da}{dN} = C \cdot \Delta K^m \qquad \text{Eq. 1}$$

where a is the crack length and N is the number of the cycles, giving da/dN the discrete crack extension/growth per cycle. C and m on the right-hand side of the equation are constants that depend on the material and the testing conditions, while ΔK is the range of the stress intensity factor experienced by the cracked material during the fatigue cycles. By taking logarithms for both sides, it yields Eq. 2:

$$\log\left(\frac{da}{dN}\right) = m \cdot \log(\Delta K) + C' \qquad \text{Eq. 2}$$

in which the C' is the constant after the logarithmic operation referring to the C in Eq. 1. Engineers strongly rely on this relation when it comes to the repair time schedule planning and the lifetime estimations of components and welded structures since it is possible to relate the expected lifetime with the limits of the available crack detection with nondestructive testing techniques.

Steels are commonly used structural materials that may be affected by HE [15-18]. There are mainly two different crystal structures in steels, namely face-centered cubic (FCC) and body-centered cubic (BCC). Generally, FCC lattice can contain more H atoms while having a slower diffusion rate (approx. 10^{-11} cm^2/s in some austenitic steels [19]), while BCC lattice has a lower H solubility but a faster diffusion rate of H (approx. 10^{-5}~10^{-4} cm^2/s [20-23]). In FCC materials, up to 12 slip systems could be found, which made the deformation analysis relatively easier, and a lot of works can be found with deep understanding on the failure behaviors, for example austenitic steels [24-26], Ni alloys [27-30] and some high-entropy alloys [31-33]. However, due to the intrinsic structure of the BCC lattice, up to 48 slip systems can be found in the deformation structure, which made the analysis much more difficult than the FCC materials. Furthermore, the non-Schmid behaviors[34, 35] as well as the non-planar nature of the screw dislocations[36] makes the deformation analysis in BCC materials complicated. To understand

the basic mechanisms in BCC materials, simple model materials with well-defined materials parameters should be studied.

Fe-Si alloys contain normally several weight percent of Si in iron matrix, giving a simple ferritic structure with BCC lattice, and this material could be used as model material for different studies. There are several reasons for choosing this alloy as a model material. First of all, Si is a ferrite stabilizing element which can ensure the material contain fully ferritic structure. Secondly, Fe-Si alloys have a higher strength than pure iron, which makes the HE effect more significant since the HE effect is in general more sensitive at higher stress levels. Thirdly, the grain size of this type of alloy can be easily controlled thanks to the adequate data of the heat treatment processes. Vehoff [37-42] did intensive work on Fe-Si alloys regarding fracture, fatigue failure and HE since 1970s. It was proposed that under H_2 gaseous environment, a crack in Fe-Si single crystal can grow stably by a combined micro-cleavage and crack-tip dislocation emissions. However, due to technical limitations in the previous decades, the resolution of their observation was rather low, though giving solid background. With the modern high-resolution techniques, more studies could be done to deepen the knowledge of these topics.

This work aims at investigating the FCGR behavior of BCC metals under electrochemical H charging conditions. Fe-3wt%Si was used as model material to reveal the role that H plays during FCG and how this extrinsicates into variations of the FCGR curves. Fractographic analysis was done by scanning electron microscopy (SEM) to investigate the microscale features of the fatigue fractured specimens. The validity of the conventional Paris' law was checked both with the mechanical data and the fractography. Statistical analysis on the small-scale features was conducted to study the H effect on the fracture modes. In addition, electron channeling contrast imaging (ECCI) was conducted to investigate the dislocation structures beneath the fracture surface. These results helped to gain a better understanding of the mechanisms of H-accelerated FCG procedure in ferritic alloys.

2. Experimental

2.1. Materials and specimens

The material used in this study is Fe-3wt%Si with simple ferritic structure. The detailed chemical composition is shown in Table 1. The raw plates were rolled from three forged blocks (approx. 80 × 160 × 470 mm each) followed by 10% cold rolling plus annealing at 800 °C for three times with the last time annealing at 1050 °C and straightening. The material has a large grain size of about 300 μm to make the test condition as simple as possible. The microstructure of the investigated material is shown in Figure 2. Compact Tension (CT) specimens were cut by electron discharge machining (EDM) from the raw materials and used for the fatigue crack growth rate testing. Figure 1 shows the geometry of the specimens (as per ASTM E647 standard), with the indicated characterizations performed after the tests.

Table 1 Chemical composition of the investigated Fe-3wt%Si steel.

Element	**C**	**Si**	**Mn**	**P**	**S**	**Cr**	**Ni**	**Mo**
wt%	0.018	3.000	0.055	0.008	0.003	0.010	0.006	0.003
Element	**Cu**	**Al**	**Ti**	**Nb**	**V**	**B**	**Zr**	**Fe**
wt%	0.013	0.015	0.001	0.002	0.001	0.0002	0.0010	balance

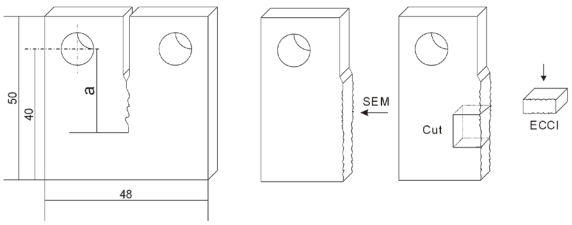

Figure 1 Geometry of the CT specimen and the microstructure of the investigated material, the crack length a is calculated from the center-line of the holes to the front of the crack tip (thickness = 8 mm). Fractography was done on the fracture surface and ECCI was done on the cross-section below the fracture surface, as indicated by the arrows.

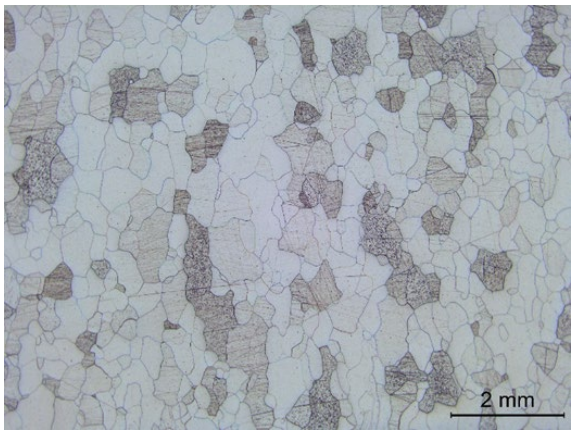

Figure 2 Microstructure of the investigated Fe-3wt%Si steel: pure ferritic structure with a grain size of about 300 µm.

2.2. Fatigue Crack Growth Rate test

The FCGR tests were carried out both in air and under in-situ electrochemical charging conditions at room temperature. The specimens were cathodically charged in a 0.1M Na_2SO_4 electrolyte with a constant potential of -1400 mV_{SCE}. Multimeters were used during the whole test in order to check the values and keep the circuit run as designed. In the electrochemical system, the specimens were used as working electrode, Pt was used as counter electrode and the reference electrode was chosen to be the saturated calomel electrode (SCE, $Hg/HgCl_2$). The FCGR test was started as soon as the electrochemistry system started running and no pre-charging was applied. Based on the classical diffusion model [43], the H can diffuse over a distance of about 10 µm (the estimated deformation zone size) within 10^{-2} s due to the relatively high diffusivity in BCC (assumed as 10^{-5} ~10^{-4} cm^2/s). It is thus assumed that the H was saturated in the plastic deformation zone ahead of the crack-tip during the whole test. The experimental setup is schematically shown in Figure 3.

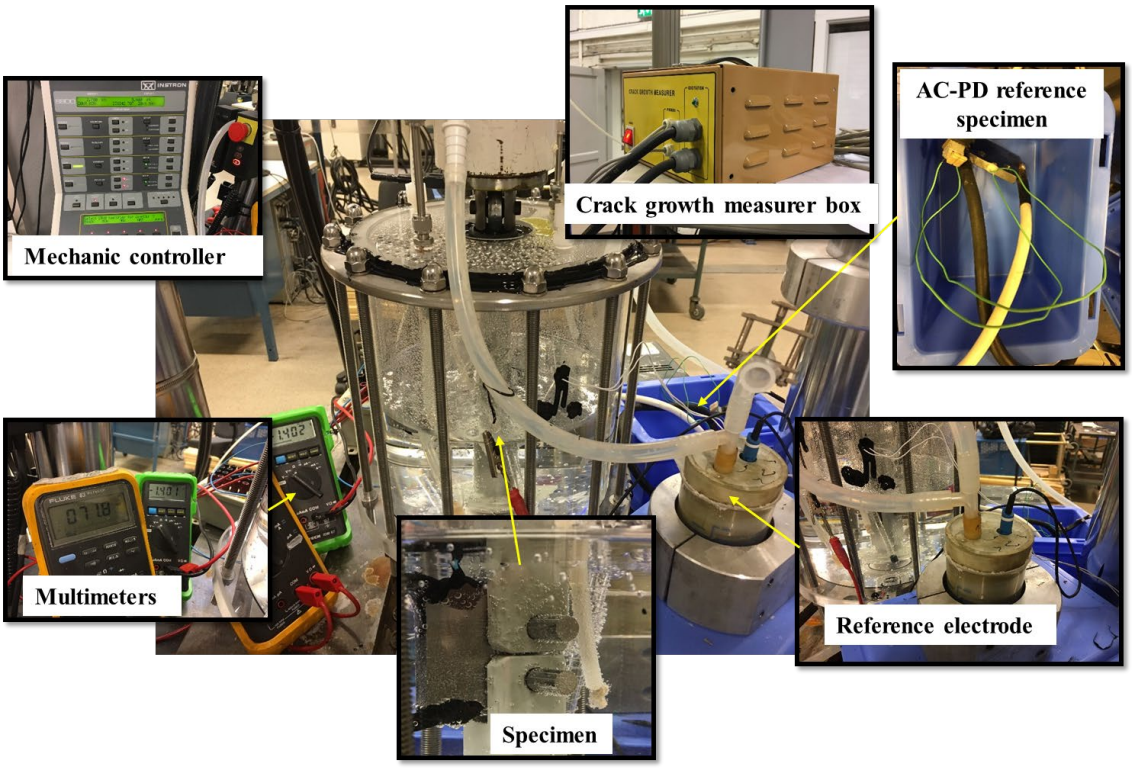

Figure 3 A schematic of the experimental setup. The key parts are pointed out.

The test frequency f was chosen to be 0.1 Hz, 1 Hz and 10 Hz. The load ration $R = 0.5$ was adopted to reduce the crack closure effect. The crack length a was measured from the center of the holes (where the load was applied) to the crack tip, as shown in Figure 1. Before tests, a pre-crack was produced by fatigue according to the procedure described in Ref.[44]. First, a lower bound threshold stress intensity factor, i.e. ΔK_{th}, ranging from 10-12 MPa$\sqrt{m}$ was used to initiate the crack from the notch. Then a reduction in the ΔK value of 5% was adopted stepwise until the target K-value was reached, and the crack growth stabilized. Typically, these pre-cracks were in the range of 2~4 mm after approximately 500 000 cycles for this material. It should be noted that after pre-cracking, most of the specimens presented the typical "fingernail" shapes in the fracture surface inherent to the different stress state and stress triaxiality through the specimen's thickness. The start and stop position measurements were therefore obtained by averaging nine points taken along the crack front. To get the crack further growing, a 5% increase in the ΔK from the last step of pre-cracking procedure was used in order to minimize the effect of the plastic zone from the pre-cracking procedure present ahead of the crack. An alternate current-potential drop (AC-PD) crack growth rate measure box was used during the whole test to record the crack growth. At the end of the test the specimens were cracked in liquid nitrogen and the da/dN vs ΔK curves were obtained from start/stop surface measurements. By integrating the crack growth data from the AC-PD measurement over the number of cycles, the crack length can be correlated to the number of cycles, which in turn, provides the ΔK information along the crack path.

2.3. Characterization

Post-mortem SEM fractographic characterization was performed on all the fractured specimens. The FEG Quanta 650 SEM (Thermo Fisher Scientific Inc., USA) was operated at 20 kV acceleration voltage with an aperture size of 50 μm. Measurements on the fracture surfaces were done by using the in-built software. In addition, to investigate the dislocation structures below the fracture surface, Electron Channeling Contrast Imaging (ECCI) was conducted with a solid-state four-quadrant Back-Scatter Electron (BSE) detector in the same SEM on the cross-section of the specimen, as indicated by the arrows in Figure 1. It is worth noting that the observation surface of the ECCI characterization was from the mid-thickness cross-section of the broken specimen, which was experiencing more plane-strain condition during the tests. The ECCI technique adopts the backscatter electron signal and forms contrast based on the local orientation. When the grain matrix is in the channeling condition (dark contrast), the crystal defects such as dislocations, twins and stacking faults can appear as bright contrast due to the local orientation change. The resulting images look similar as the micrographs from dark-field imaging in transmission electron microscopy (TEM). This technique has shown its capability in studying HE related deformation information in a variety of materials with satisfying results [25, 45-49]. The theoretical and practical details of the ECCI technique can be found in Ref [50].

3. Results

3.1. Fatigue crack growth rate test

Fatigue crack growth rate testing on the Fe-3wt%Si were performed in air (R=0.5; f=10 Hz) and under in-situ cathodic charging conditions (R=0.5; f=0.1, 1 and 10 Hz). The resulting FCGR curves are shown in Figure 4. Additionally, some data on gaseous H_2 charged FCGR tests of pure Fe were added from Ogawa et al. [51] for reference, and this reference showed a similar mechanical performance range between these two different materials and therefore could give a validation of the tests presented in this work. However, since the charging conditions as well as the loading conditions are not exactly the same, no direct comparison between the behaviors could be made to predict the behaviors of these two different materials, and this reference is only used to show the similar degradation tendency in the mechanical performance of these two similar materials in H environment. The Fe-3wt%Si specimens tested under cathodic H-charging conditions exhibited a higher FCGR than the one tested in air. The H-enhanced acceleration featured a strong dependency with respect to the test frequency: the lower the frequency was, the more pronounced acceleration in the FCGR. The Paris' law parameters obtained from the curves were summarized in Table 2. The presence of H induced an acceleration in crack growth of about 1000 times while the low variation in m values indicated rather a shifting of the curves, i.e. the effect of H was independent on the ΔK level when focusing on the Paris' domain. It should be noted that the 1000 times acceleration was based on the frequency dependency when we compared the test with 0.1 Hz under cathodic H-charging and the reference test in air. However, if we focus on the test with 1 Hz loading frequency, the acceleration factor was about 30 times, which is approximately the same as the tests on pure Fe by Ogawa et al. [51]

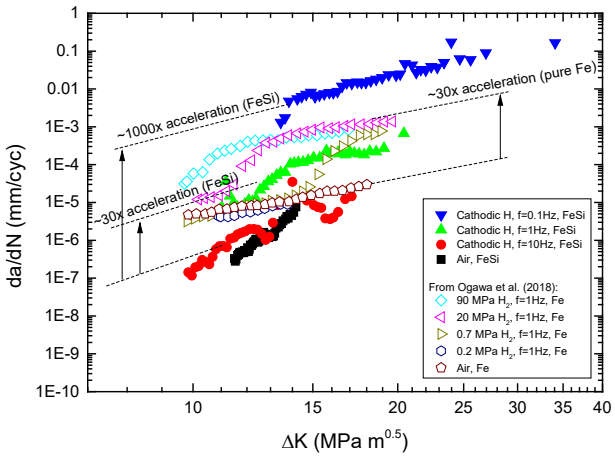

Figure 4 da/dN - ΔK curves of the investigated Fe-3wt%Si steel under different environments. The pure Fe data under gaseous H_2 charging conditions were adopted from Ogawa et al. [51] for comparison.

Table 2 The fitted Paris' parameters of the investigated Fe-3wt%Si steel.

Test condition	*C'*	*m*
Air, *R*=0.5, *f*=10 Hz	3E-17	7.890
H, *R*=0.5, *f*=10 Hz	3E-15	7.898
H, *R*=0.5, *f*=1 Hz	5E-13	6.986
H, *R*=0.5, *f*=0.1 Hz	7E-9	5.048

3.2. Statistical analysis on fractography

When it came to the fractography analysis, three different regions were identified for each specimen (see Figure 5a): the EDM region, the fatigue pre-cracked region and the stable FCG region. In order to have a consistent and reliable measurement methodology, 1 mm from the measured "start" and "stop" line was removed as well as from the specimen flanks: only the central part enclosed by yellow dashed lines was considered for detailed fractography analysis. This region was schematized through a 0.6 mm grid and the features at the nodes were considered as representative of the mechanism and taken into statistics by their area fraction. The fractographic features were, according to their main appearances, divided in three different categories: transgranular (TG), intergranular (IG) and "quasi-cleavage" (QC) features. TG zones are characterized by the traditional ductile striation whose main directions are mostly aligned with the global crack growth testing direction (see Figure 5b). IG features reveal grain-boundary-like surfaces (see Figure 5c) while "QC" features are normally showing facets and smooth area between striations, sometimes accompanied by river-marks (Figure 5d). It is worth noting that the "QC" features are different than the pure cleavage fracture features. Cleavage features are normally flat and featureless fracture surfaces or contain some river-marks. And the cleavage features are always strictly along some specific crystallographic planes (in the case of BCC materials, along {100} planes). The "QC" features, however, are not strictly along such planes.

The statistical distribution of the aforementioned fracture zones within the specimens tested under H-charging conditions were plotted in Figure 6 against the ΔK level over the whole tested area (Figure 6a) and focusing at a common ΔK range for all three specimens (Figure 6b) to ease a direct comparison. It is evident that the fracture modes are quantitatively strongly dependent on the test frequency and the ΔK level. When the ΔK level increased, the fracture mode changed from TG to "QC", while IG type fracture took only a small fraction and did not change significantly. The same trend could be observed when the load frequency became lower. When focusing at the same ΔK level, a lower frequency gave a higher fraction of "QC" fracture and a smaller fraction of TG fracture, but IG type fracture remained similar for all frequencies by a minor fraction.

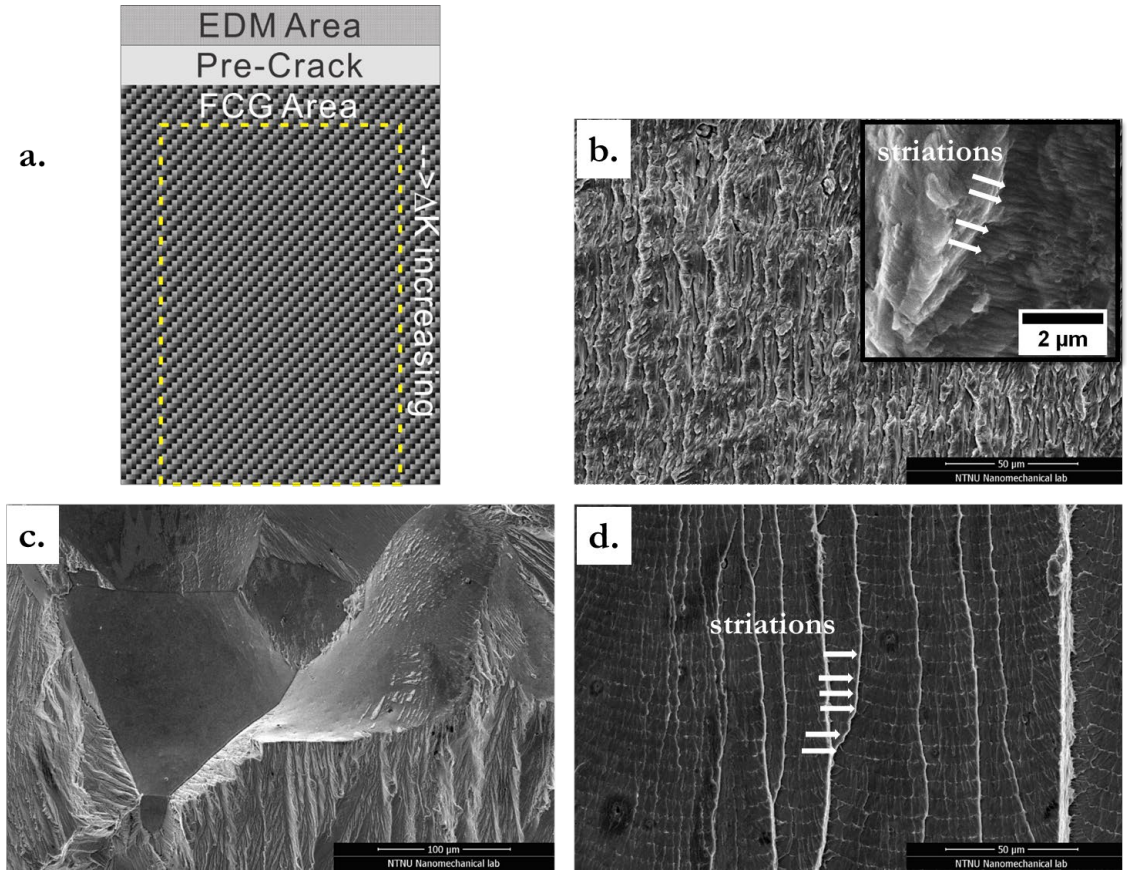

Figure 5 ***a****. schematic description of the statistical analysis;* ***b****. typical TG fracture surface with a close-up sub-figure;* ***c****. typical IG fracture surface;* ***d****. typical "QC" fracture surface. The striations are highlighted by white arrows.*

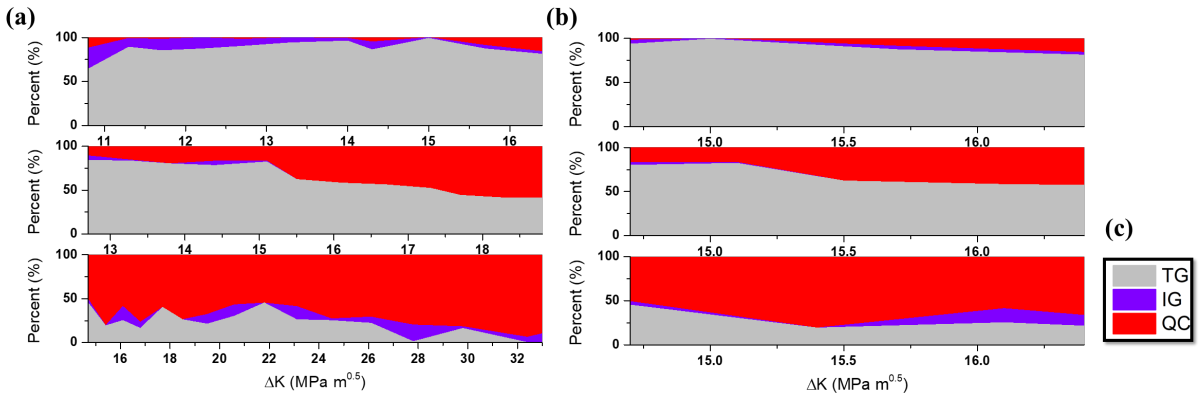

Figure 6 Fracture mode statistical distribution vs. ΔK level (a) over the whole tested area and (b) focusing at the same ΔK range. (c) is the legend for all plots.

The analysis of the striation morphology exhibited in the different specimens indicates a different striation appearance in relation to the different fracture modes and depending on the environmental conditions. Striations from TG zones are denser and deeper (Figure 7) indicating a strong plastic development in front of the crack during the load cycle and the crack advance while the ones featured in the "QC" fracture zones are sparser (Figure 8), and with much smaller crests. In IG zones, no striations were observed (Figure 9).

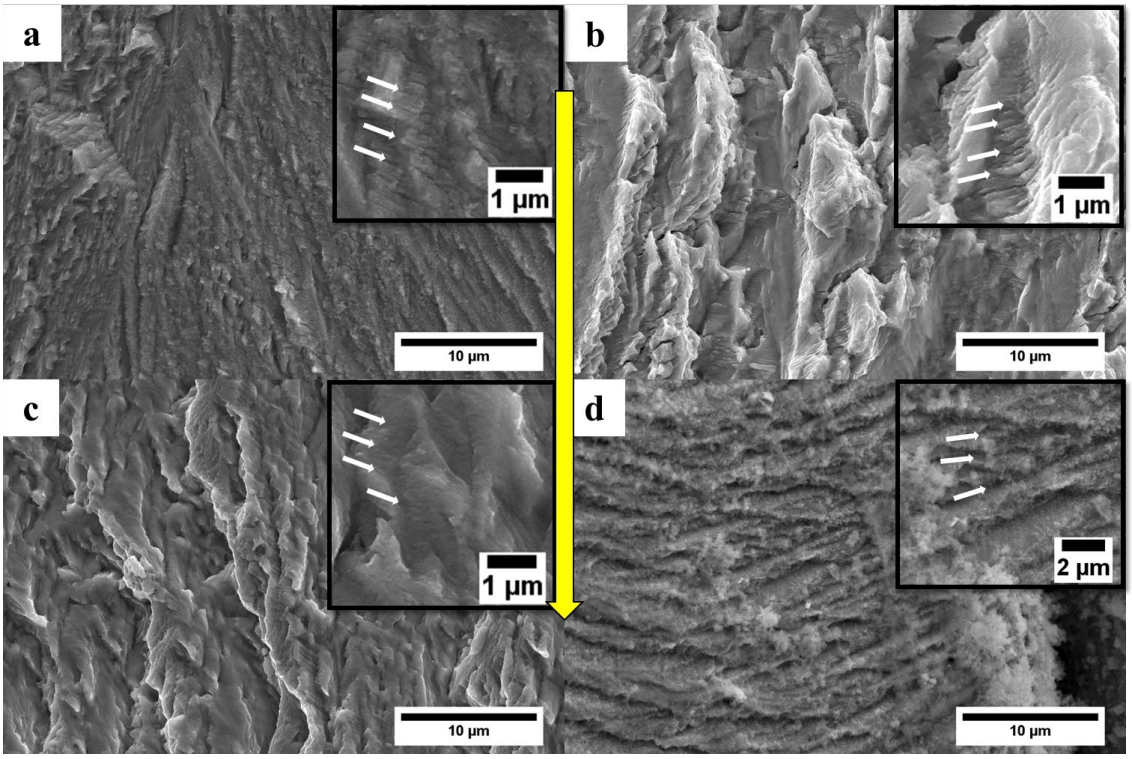

*Figure 7 Fatigue striations in TG fracture zones with corresponding magnified subsets (**a**. in Air; **b**. in H, f = 10 Hz; **c**. in H, f = 1 Hz; **d**. in H, f = 0.1 Hz). The yellow arrow shows the global fatigue crack growth direction. White arrows show the striations.*

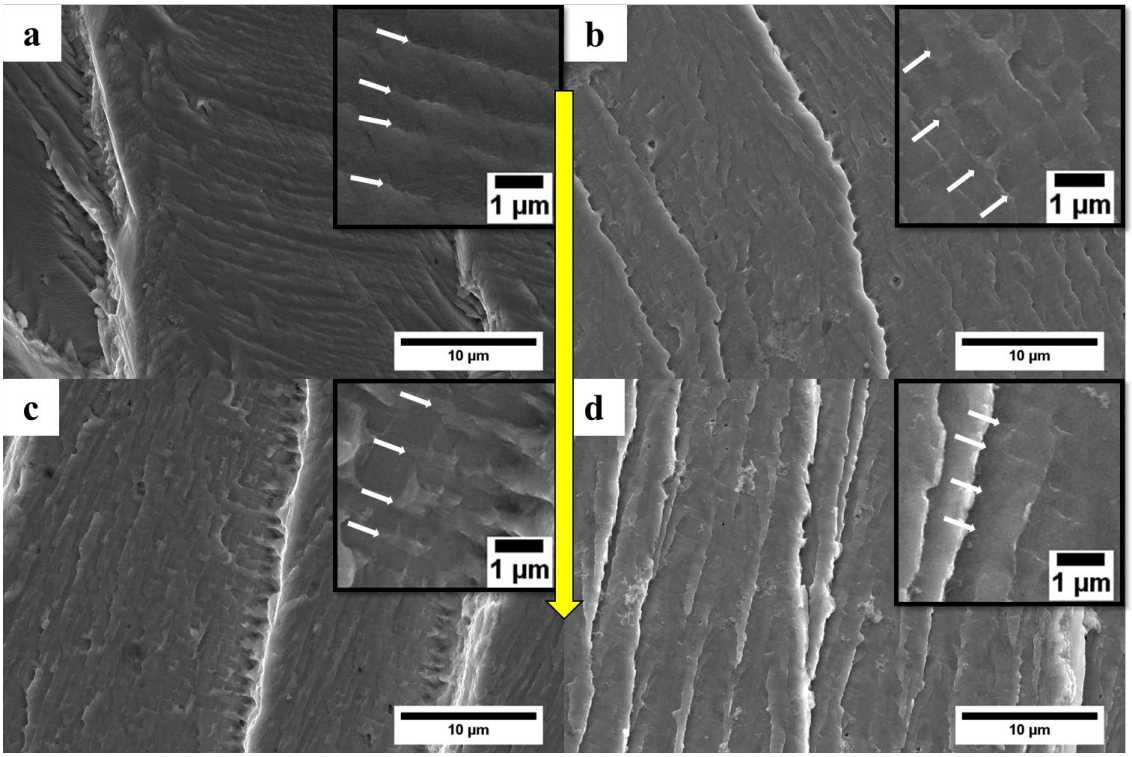

*Figure 8 Fatigue striations in "QC" fracture zones with corresponding magnified subsets (**a**. in Air; **b**. in H, f = 10 Hz; **c**. in H, f = 1 Hz; **d**. in H, f = 0.1 Hz). The yellow arrow shows the global fatigue crack growth direction. White arrows show the striations.*

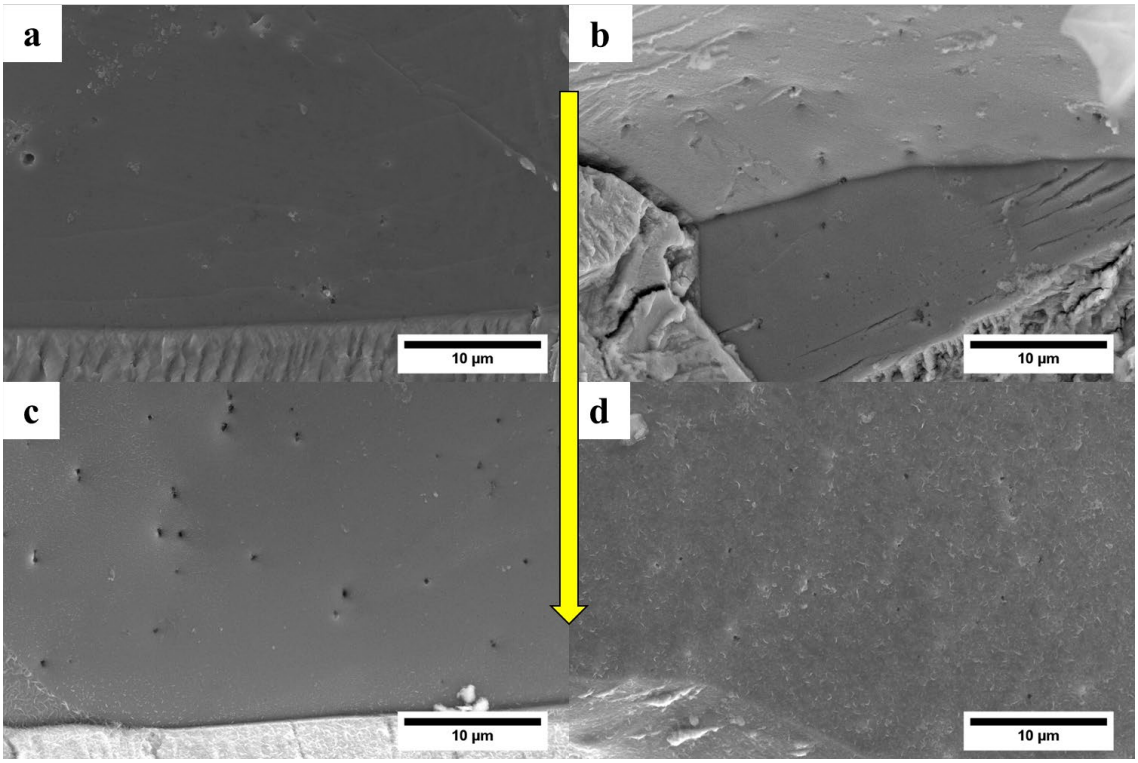

*Figure 9 IG fracture zones (**a**. in Air; **b**. in H, f = 10 Hz; **c**. in H, f = 1 Hz; **d**. in H, f = 0.1 Hz). The arrow shows the global fatigue crack growth direction.*

3.3. Dislocation structures

ECCI investigations were performed for both H-free (reference air test) and H-charged (the most significantly accelerated condition at f=0.1 Hz) conditions at similar ΔK levels in order to unveil the dislocation structures below the fracture surface. The H-free cases consist of fracture features only in TG manner, thus the area below the TG feature in the H-charged case which experienced the same ΔK level were also subjected to investigation for the sake of comparison. The preliminary results are shown in Figure 10. Clearly, a plastic zone can always be observed under the fracture surface, meaning the FCG procedure was accompanied by plastic deformation mechanisms, but the plastic zone has a different appearance between the specimens with and without H-charging. At the investigated common ΔK level (14~17 MPa$\sqrt{m}$), the air tested specimen always shows dislocation cells that were emanated from the fracture surface. The dislocation density became lower when it goes further from the fracture surface, but the majority of dislocations tend to form highly-densed dislocation walls (HDDWs) in the investigated areas. On the contrary, although a plastic zone was also observed under the fracture surface of the H-charged specimen, the dislocations did not prefer to form well-structured walls but rather distributed individually or at least less organized. At the highest ΔK level investigated (17 MPa$\sqrt{m}$), the dislocations in the H-charged specimen started to organize, but only a single tangling direction could be seen, as shown in Figure 10f, and no complete dislocation cells could be observed. These results showed a convincing proof of the H effect on the dislocation activities during FCG.

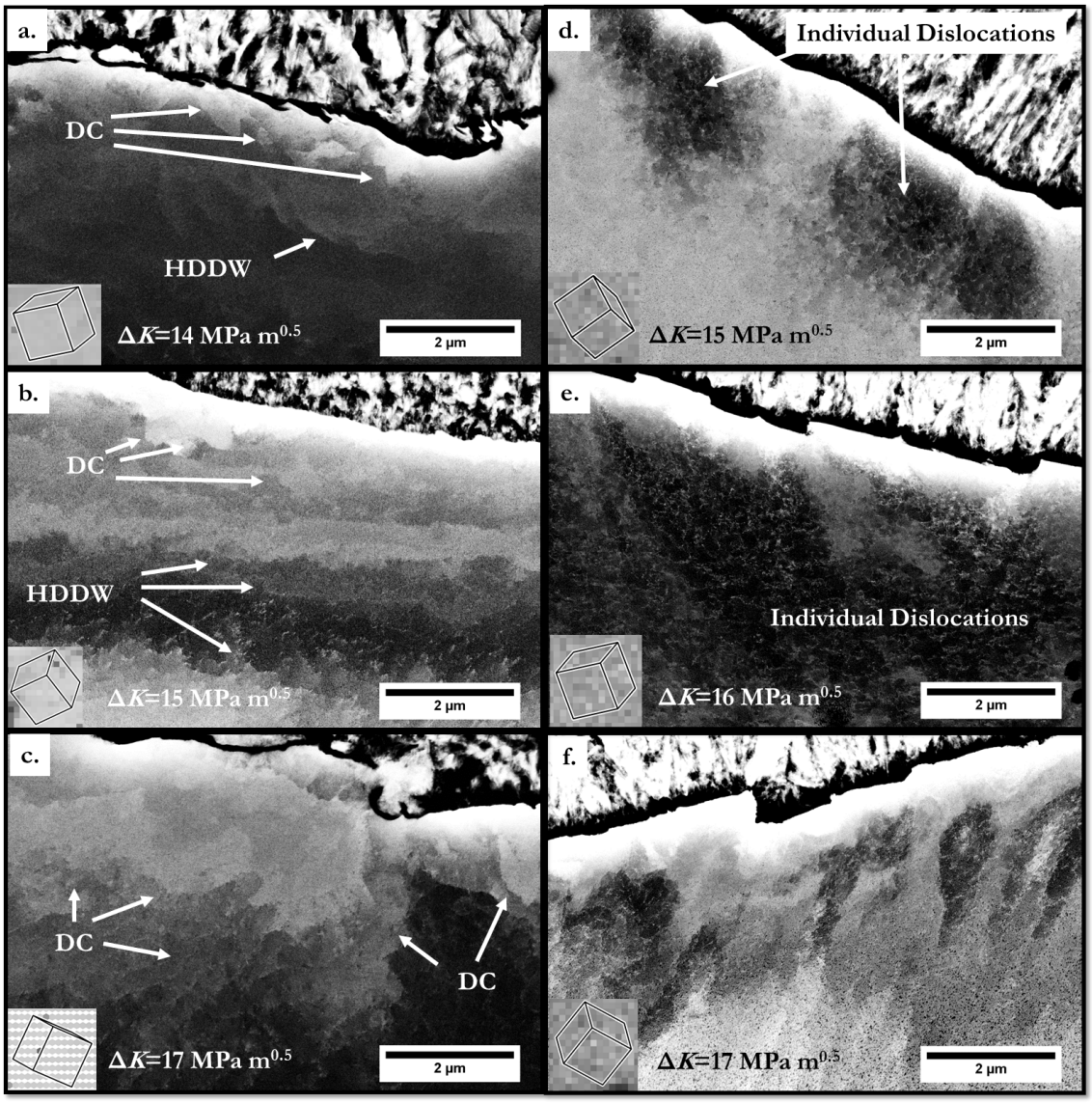

*Figure 10 Dislocation structures below the fracture surface after FCGR testing with features highlighted (**a-c**. reference test in air; **d-f**. with cathodic H-charging, R=0.5, f=0.1 Hz). DC: dislocation cell. HDDW: highly densed dislocation wall. The global FCG direction is from left to right. The ΔK levels and representative unit cells are indicated in each sub-figure.*

4. Discussion

4.1. Paris' law

The Paris' relation was used to describe the FCG behavior at macroscale viewpoint in coincidence with the linear regime or stable crack growth regime, just as shown in Figure 4. A general phenomenon is that "QC" type fracture gave a faster crack growth rate (higher *da/dN* value) while that for TG type fracture was slower (lower *da/dN* value). The shift from a TG to "QC" mechanism determined the enhanced FCGR in presence of H as the testing frequency was decreased from 10 Hz to 0.1 Hz.

For FCG tests in Air, the fracture mode could remain similar all over the specimen without strong change in mechanism, and the parameters in the Paris' relation could be linked more easily to the fracture feature (*da/dN*). Therefore, the Paris' law holds the mathematically simple linear relation for most of the crack path. However, when tested in H environment, the fracture mode was changed by the effect of H, which determined the local fracture mechanism and consequently the appearance of the fracture surface, and thus, it cannot be simply described by the single mathematical relation. That is to say, it is difficult to link the microstructural features to the Paris' parameters. To the authors' knowledge, there is no report correlating the Paris' parameters to the dislocation activities, especially with H influence. However, since the global FCGR is an averaged value over a large area comparing to single striations, the Paris' law still holds at the continuum level.

Hence, it can be concluded that the Paris' law can describe the global mechanical FCG data in a satisfactory manner, but it is difficult to describe the local FCG behavior at microscale, especially when special environmental conditions apply.

4.2. FCGR behavior in air

The *da/dN* - *ΔK* curve showed a typical Paris' regime of the specimen tested in Air environment. The general features in the fracture surface are mainly TG type, revealing good ductility of this material. These findings are consistent with most other studies on the similar Fe-Si alloy system [37-41, 52-54]. A rather limited fraction of IG type fracture indicated that grain boundaries (GBs) were not significant vulnerable places for this material when subjected to H environment. This was confirmed in a previous work by Hajilou et al. [55] that the GB in Fe-3wt%Si was not a favored path for crack growth after their test of bending a micro-cantilever with a notch on a GB. They found that the crack generated from the notch would rather propagate along the direction with the highest degree of stress concentration rather than along the GB, whether in vacuum or in H environment. When the GB was placed beneath the notch (technically, it was the notch fabricated above the GB), the position of stress concentration could be influenced by the GB, while the crack still extended following the concentration direction but not exactly the GB direction. From this investigation, it can be concluded that the GB of this material is not the preferred cracking path under monotonic loading and is not sensitively susceptible to HE, such that the crack cannot propagate via the interface opening mechanism. Since fatigue crack generally grows via ductile mechanisms even along a microstructural interface, it is reasonable to think that IG fracture is even more difficult in the FCGR testing. Furthermore, the dimension of the micro-cantilever testing in [55] can roughly present the case of a single cycle in the present FCGR testing. From these aspects, it is assumed that the GB in the investigated material has a relatively good resistance against IG cracking both in H-free and in H-charged environments. This assumption agrees well with the fractography analysis that the IG feature fraction was not changed significant with different H-charging conditions.

4.3. H-affected fatigue crack growth rate

In the H-charged specimens, the distance between fatigue striations was measured and verified with the global *da/dN* data from the FCGR test. When measuring the distances, a specific area with a certain ΔK value was located, and a line was drawn along the direction perpendicular to the striations (referring to the local crack growth direction). The distance between striations was then calculated to be the length of the line over the number of striations (normally around 20 striations were counted per measurement). For each specific ΔK value, at least five different

areas with clear striations were measured to reduce the occasional error. It is found that the distance between striations (considered as the local crack extension per cycle, *da/dN*) in the "QC" fracture zones is always several times higher than the globally measured *da/dN* data, while that in the TG fracture zones is approximately the same or a little bit smaller than the measured global *da/dN* data, independent of the testing frequency. The measurement was subjected to the same ΔK range and the result is shown in Figure 11. It suggests that the different fraction of the "QC" feature should be responsible for the global enhancement of the FCGR. And the fraction of the "QC" has a dependency on the loading frequency. In the studied loading frequency range (0.1 ~ 10 Hz), a lower frequency gives a larger fraction of the "QC" features. IG type fracture was also not so common in H-charged specimens, suggesting that GB is not the most critical material feature with respect to HE in this material.

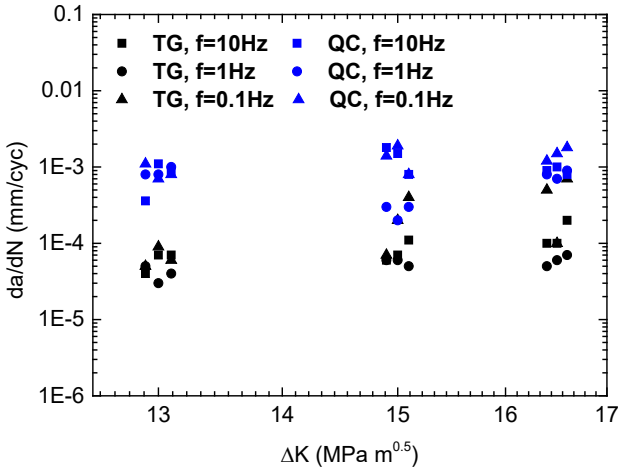

Figure 11 Striation distance vs. ΔK level in different fracture modes.

It has been observed in other works that H can change the fatigue fracture mode from ductile striations to brittle cleavage facets. Marrow et al. [56] discussed this phenomenon intensively in 1992. They proposed that H can be trapped to the intensive stress field ahead of the crack tip, arresting the sharp cleavage crack and blunting the crack. This procedure will be repeated during cyclic loading and make the cleavage fracture surface shown as facets. Vehoff [40] observed similar structures in Fe-2.6%Si single crystals. It is considered that under gaseous H_2 environment, the crack grows stably in a stepwise micro-cleavage manner as well as through enhanced dislocations emission from the crack tip. This was proposed to explain the sharp cleavage fracture structure. Several works have observed similar features in low carbon steels [57-59] and Fe-Si alloys [60], subjected FCG tests in H_2 gaseous environments. Most of these proposals were based on the cleavage fracture behavior. In this work, however, no solid proof showed the cleavage fracture manner. According to the grain orientation information shown in Figure 10, the fracture surfaces were not consistently parallel to the cleavage {100} planes of the grains. One reason could be that the H concentration produced by the in-situ cathodic charging was not high enough to activate the cleavage fracture manner of this material. To prove this hypothesis, the diffusion condition and electrochemical processes should be analyzed in detail, and this analysis will be conducted in a future work.

Similar tests on pure iron and low carbon steels were done recently in a similar manner subjected to gaseous H_2 environment [61, 62]. The fracture behaviors were identical to what was observed in the present study. It was explained that H can be transported by mobile dislocations based on the hypothesis of the HELP mechanism [5, 63], and the formation of dislocation tangles can give a local enhancement of the H concentration, leading to H-assisted cracking. This description seemed to be a "black box" in explaining the formation of the "QC" fracture feature. Basically, they linked the more brittle "QC" fracture feature directly to the local H concentration. Under this assumption, more "QC" fracture should be observed along the dislocation cell boundaries since more H was trapped there. According to the dislocation structure characterization results in the present work (Figure 10), the dislocations became less tangled when H was charged, meaning that H did affect the deformation structures during FCG. This effect of H agreed with a previous report on Ni [3]: when H was introduced to the Ni specimen, the dislocations moved out of the cell wall into the cell matrix within two seconds upon 150 torr gaseous H_2 charging. One possible mechanism could be that H tried to stop the dislocation sub-structure evolution during deformation, and the crack blunting by dislocation motion was suppressed and thus the crack became sharper. According to the basic linear elastic fracture mechanics theory, sharper cracks could make the local stress intensity higher and consequently, a faster crack growth could be expected.

Now attention should be paid to why the dislocation structure was changed by H. One possible explanation put forward by Wang et al. [4] was that the presence of H would enhance the velocity of dislocations, as already confirmed in some previous works by means of in-situ TEM with the help of environmental cells [7]. The attachment of H atoms to the dislocations would change the local stress field of the dislocations, resulting in the enhancement of dislocation mobility in some directions while suppressing the motion in other directions. Consequently, the dislocation celling procedure could not be realized but instead, more isolated dislocations in specific directions should be observed. This explanation agreed with the present results in Figure 10. However, the present results could not give a comprehensive understanding on the influence of H on the specific dislocation motion directions due to several reasons. Firstly, the investigated material was a large-grained polycrystalline material so that the local stress state could be different from place to place at grain scale. Secondly, the tested specimen experienced different stress state through the thickness direction. The investigated results were from the mid-thickness cross-section that experienced more plane-strain condition, which might give some difference to other works since most researches were focusing on the surface area which had more plane-stress condition. Thirdly, the diffraction condition of the ECCI investigations in this work was not under fully control, and some crystallographic directions in the images were not indexed. To solve these problems, new study by using single crystalline specimens with defined stress condition combined with high-resolution TEM technique was encouraged. Due to technical limitations, this could not be realized in this work.

It is interesting to note that although a similar mechanical performance (c.f. Figure 4) was observed on pure Fe [51], the dislocation structures, however, showed strongly different appearances as to the present study. The major dislocation structures in pure Fe in Ref. [51] were dislocation cells independent on the H-charging conditions, while in the investigated Fe-3wt%Si steel, dislocation cells appeared only in the air tested specimen. Several reasons could contribute to this difference. Firstly, pure Fe is mechanically softer than Fe-3wt%Si since the Si, as a substitutional element, hardens the matrix by solid solution hardening mechanism [64]. Under the same load, the dislocations in the softer pure Fe could be organized into cells more

easily than in the harder Fe-3wt%Si steel since the dislocation motion in softer materials is more pronounced than in harder materials. When H was charged into the system, the matrix could further be hardened by H atom since this element could serve as interstitial element and cause solid solution strengthening. As a result, the H-charged specimen might have less possibility in the dislocation cell formation. Secondly, the dislocation cell formation is strongly associated with dislocation activities that depend on the stacking fault energy (SFE), for example the cross-slip and climbing procedures. A general rule is that when the SFE is high, dislocations are easily remained as full dislocations during deformation and the cross-slip and climbing procedures are more pronounced. As a result, dislocations cells could be formed more easily [43]. Regarding the present study, the SFE of ferrite was reduced by adding Si [65]. Therefore, the Fe-3wt%Si steel was expected to have less cell formation than the pure Fe due to this SFE difference. If we focus on the H-free case for both of these two works, the present Fe-3wt%Si showed the cell formation up to about 5 μm under the fracture surface, while the pure Fe in [51] showed all features as dislocation cells through the investigation range of more than 10 μm. From this comparison, it might be inferred that the SFE played a role in the dislocation structure formation. By simply adding Si or H into the system, the dislocation sub-structure did not change significantly. Nevertheless, when both Si and H were introduced, the dislocation cells disappeared. Since both Si and H have the effect of decreasing the SFE of the system, this could be considered as a reason for this evolution. To prove this proposal, researchers working in the numerical methods are encouraged to give a contribution since it is technically challenging for the experimentalists. Thirdly, we showed the results with respect to the loading frequency change while the results in [51] mainly focused on the amount of H by changing the H_2 gas pressure. Although both cases could give the dependency on the H amount, the mechanisms of H-uptake were different. Furthermore, the results of H-charged specimen in Figure 10 were from the test at f=0.1 Hz, while the results in [51] were mainly from the tests at f=1 Hz, by which comparison it could make the H-uptake difference even more significant. From the mechanical behavior, the Fe-3wt%Si in the present work showed a more pronounced acceleration in the FCGR (up to 1000x) than the pure Fe in [51] (up to 30x), and this might indicate that the H was influencing the Fe-3wt%Si more severely than the pure Fe in Ref [51] under the tested conditions. Hence, it could be inferred that the different dislocation structures came from the different H amount: a more significant H influence could lead to less dislocation cell formation. In summary, the dislocation structure difference between Fe-3wt%Si and pure Fe could be reasoned as the influence from strength, SFE and H-charging. Nevertheless, the difference in the H fugacity in different materials as well as under different charging conditions could give contribution to the deformation structure evolution and due to limitations in the techniques and time, only qualitative comparisons could be provided in the present work. For more detailed quantitative analysis, researchers in the field of numerical methods and with more advanced devices are encouraged to shed some light on this topic.

4.4. Frequency effect

The fracture modes as a function of ΔK level and crack propagation for different frequencies were measured as described in 3.2 and the resulting map is shown in Figure 6. It is clearly shown in this map that the frequency of the fatigue test yields strong change in the fracture modes. When a low frequency (0.1 Hz) was applied, the “QC” type dominated in the fracture surface, and when a high frequency (10 Hz) was applied, the TG type dominated, while an intermediate frequency (1 Hz) gives the result in between. In other words, the lower the test frequency, the more the time for H to diffuse toward the highly stressed zone at the crack tip,

the more pronounced is the measured acceleration in the FCGR. Since the diffusivity of H in BCC structure is commonly considered as high (diffusion coefficient of H in α-Fe is about 10^{-5}~10^{-4} cm^2/s, according to Refs [20-23]), such that the time for H diffusion into the deformation structure is short enough to be neglected, the procedure of H interaction with deformation structure is considered as a time-dependent process.

5. Conclusions

The effect of H on fatigue crack growth behavior in a Fe-3wt%Si alloy under in-situ electro-chemical H charging condition was studied. The fracture modes distribution was statistically summarized along the crack growth path and the effect of testing frequency on the fracture mode transition was discussed. Some conclusions are drawn as follows:

- The H-assisted FCGR was revealed by means of in-situ cathodic charging on a Fe-3wt%Si steel. The H-charging could enhance the FCGR by up to 1000 times compared to the reference test in lab air, depending on the test frequency.
- The Paris' law could satisfactorily describe the FCGR behavior of a specimen at continuum level but cannot precisely describe the local behavior at microstructure level, especially when special environmental conditions applied.
- Post-mortem fractography clearly showed a shift in crack growth mechanisms: the FCG mode of the investigated material changed from TG to "QC" type; IG type fracture was not common in this material, indicating that the GB in this material was not the preferred path for crack propagation.
- The investigated dislocation structures below the fracture surface suggested that H can give a negative effect on the dislocation cell formation. This phenomenon was explained by the enhancement of dislocation mobility in specific directions.
- The test results confirmed the time-dependent nature of the H-deformation interaction: in the tested frequency range (0.1 Hz – 10 Hz) in H environment, a lower frequency would lead to more significant enhancement of the FCGR.

An ideal prospect would be an in-situ investigation on a specimen with most parameters well-defined. This has been planned by the present authors and would be realized in a future work.

Acknowledgement

This work was financially supported by the Research Council of Norway (Petromaks2 Program, Project No. 244068/E30, HyF-Lex).

Reference

[1] Hirth JP. 1980 Institute of Metals Lecture the Metallurgical-Society-of-Aime - Effects of Hydrogen on the Properties of Iron and Steel. Metallurgical Transactions a-Physical Metallurgy and Materials Science. 1980;11:861-90.
[2] Robertson IM, Birnbaum HK, Sofronis P. Hydrogen Effects on Plasticity. In: Hirth JP, Kubin L, editors. Dislocations in Solids. first ed. Amsterdam: Elsevier; 2010. p. 249-93.

[3] Robertson IM, Birnbaum HK. An Hvem Study of Hydrogen Effects on the Deformation and Fracture of Nickel. Acta Metall. 1986;34:353-66.
[4] Wang S, Nagao A, Sofronis P, Robertson IM. Hydrogen-modified dislocation structures in a cyclically deformed ferritic-pearlitic low carbon steel. Acta Mater. 2018;144:164-76.
[5] Beachem CD. A new model for hydrogen-assisted cracking (hydrogen "embrittlement"). Metall Mater Trans B. 1972;3:441-55.
[6] Birnbaum HK, Sofronis P. Hydrogen-enhanced localized plasticity—a mechanism for hydrogen-related fracture. Mater Sci Eng, A. 1994;176:191-202.
[7] Robertson IM. The effect of hydrogen on dislocation dynamics. Eng Fract Mech. 1999;64:649-73.
[8] Gangloff RP. Critical issues in hydrogen assisted cracking of structural alloys. In: Shipilov SA, Jones RH, Olive J-M, Rebak RB, editors. Environment-Induced Cracking of Materials. Amsterdam: Elsevier; 2008. p. 141-65.
[9] Gerberich WW, Marsh PG, Hoehn JW. Hydrogen Induced Cracking Mechanisms - Are There Critical Experiments? In: Thompson AW, Moody NR, editors. Hydrogen Effects in Materials. Warrendale, Pennsylvania, USA: Minerals, Metals & Materials Society (TMS); 1996. p. 539-54.
[10] Oriani RA. Whitney Award Lecture—1987:Hydrogen—The Versatile Embrittler. Corrosion. 1987;43:390-7.
[11] Oriani RA, Josephic PH. Equilibrium and kinetic studies of the hydrogen-assisted cracking of steel. Acta Metall. 1977;25:979-88.
[12] Lynch SP. Environmentally Assisted Cracking - Overview of Evidence for an Adsorption-Induced Localized-Slip Process. Acta Metall. 1988;36:2639-61.
[13] Bilotta G, Henaff G, Halm D, Arzaghi M. Experimental measurement of out-of-plane displacement in crack propagation under gaseous hydrogen. Int J Hydrog Energy. 2017;42:10568-78.
[14] Peralta P, Laird C. Fatigue of Metals. In: Laughlin DE, Hono K, editors. Physical Metallurgy (Fifth Edition). Amsterdam: Elsevier; 2014. p. 1765-880.
[15] Depover T, Laureys A, Perez Escobar D, Van den Eeckhout E, Wallaert E, Verbeken K. Understanding the Interaction between a Steel Microstructure and Hydrogen. Materials (Basel). 2018;11.
[16] Depover T, Pérez Escobar D, Wallaert E, Zermout Z, Verbeken K. Effect of hydrogen charging on the mechanical properties of advanced high strength steels. Int J Hydrog Energy. 2014;39:4647-56.
[17] Depover T, Verbeken K. Evaluation of the role of Mo2C in hydrogen induced ductility loss in Q&T FeCMo alloys. Int J Hydrog Energy. 2016;41:14310-29.
[18] Depover T, Verbeken K. Hydrogen trapping and hydrogen induced mechanical degradation in lab cast Fe-C-Cr alloys. Mater Sci Eng, A. 2016;669:134-49.
[19] Kanezaki T, Narazaki C, Mine Y, Matsuoka S, Murakami Y. Effects of hydrogen on fatigue crack growth behavior of austenitic stainless steels. Int J Hydrog Energy. 2008;33:2604-19.
[20] Wang S, Hashimoto N, Ohnuki S. Effects of hydrogen on activation volume and density of mobile dislocations in iron-based alloy. Mater Sci Eng A. 2013;562:101-8.
[21] Araújo DF, Vilar EO, Palma Carrasco J. A critical review of mathematical models used to determine the density of hydrogen trapping sites in steels and alloys. Int J Hydrog Energy. 2014;39:12194-200.
[22] Lynch S. Hydrogen embrittlement phenomena and mechanisms. Corros Rev. 2012;30:105-23.
[23] Bruzzoni P, Carranza RM, Collet Lacoste JR, Crespo EA. Hydrogen diffusion in α-iron studied using an electrochemical permeation transfer function. Electrochim Acta. 1999;44:2693-704.
[24] Koyama M, Akiyama E, Sawaguchi T, Ogawa K, Kireeva IV, Chumlyakov YI, et al. Hydrogen-assisted quasi-cleavage fracture in a single crystalline type 316 austenitic stainless steel. Corros Sci. 2013;75:345-53.

[25] Koyama M, Springer H, Merzlikin SV, Tsuzaki K, Akiyama E, Raabe D. Hydrogen embrittlement associated with strain localization in a precipitation-hardened Fe-Mn-Al-C light weight austenitic steel. Int J Hydrog Energy. 2014;39:4634-46.
[26] Koyama M, Yamamura Y, Che RQ, Sawaguchi T, Tsuzaki K, Noguchi H. Comparative study on small fatigue crack propagation between Fe-30Mn-3Si-3Al and Fe-23Mn-0.5C twinning-induced plasticity steels: Aspects of non-propagation of small fatigue cracks. Int J Fatigue. 2017;94:1-5.
[27] Demetriou V, Robson JD, Preuss M, Morana R. Study of the effect of hydrogen charging on the tensile properties and microstructure of four variant heat treatments of nickel alloy 718. Int J Hydrog Energy. 2017;42:23856-70.
[28] Yu HY, Olsen JS, Olden V, Alvaro A, He JY, Zhang ZL. Cohesive zone simulation of grain size and misorientation effects on hydrogen embrittlement in nickel. Eng Fail Anal. 2017;81:79-93.
[29] Zhang ZB, Obasi G, Morana R, Preuss M. Hydrogen assisted crack initiation and propagation in a nickel-based superalloy. Acta Mater. 2016;113:272-83.
[30] Carroll MC, Carroll LJ. Developing Dislocation Subgrain Structures and Cyclic Softening During High-Temperature Creep–Fatigue of a Nickel Alloy. Metall Mater Trans A. 2013;44:3592-607.
[31] Luo H, Li Z, Lu W, Ponge D, Raabe D. Hydrogen embrittlement of an interstitial equimolar high-entropy alloy. Corros Sci. 2018;136:403-8.
[32] Zhao Y, Lee D-H, Lee J-A, Kim W-J, Han HN, Ramamurty U, et al. Hydrogen-induced nanohardness variations in a CoCrFeMnNi high-entropy alloy. Int J Hydrog Energy. 2017;42:12015-21.
[33] Li Z, Raabe D. Influence of compositional inhomogeneity on mechanical behavior of an interstitial dual-phase high-entropy alloy. Mater Chem Phys. 2017.
[34] Taylor GI, Elam CF. The Distortion of Iron Crystals. Proc R Soc London, Ser A. 1926;112:337-61.
[35] Christian JW. Some surprising features of the plastic deformation of body-centered cubic metals and alloys. Metall Mater Trans A. 1983;14:1237-56.
[36] Vitek V, Mrovec M, Bassani JL. Influence of non-glide stresses on plastic flow: from atomistic to continuum modeling. Mater Sci Eng, A. 2004;365:31-7.
[37] Vehoff H. Untersuchung der duktilen und quasispröden zyklischen Rißausbreitung in Fe-3%-Si-Einkristallen. Aachen: RWTH Aachen; 1977.
[38] Vehoff H, Neumann P. In situ sem experiments concerning the mechanism of ductile crack growth. Acta Metall. 1979;27:915-20.
[39] Vehoff H, Neumann P. Crack propagation and cleavage initiation in Fe-2.6%-Si single crystals under controlled plastic crack tip opening rate in various gaseous environments. Acta Metall. 1980;28:265-72.
[40] Vehoff H, Rothe W. Overview .30. Gaseous-Hydrogen Embrittlement in Fesi-Single and Ni-Single Crystals. Acta Metall. 1983;31:1781-93.
[41] Vehoff H. Rißbildung und Rißausbreitung in Ein- und Bikristallen. Düsseldorf1994.
[42] Vehoff H, Nykyforchyn A. Fatigue crack nucleation at grain boundaries – experiment and simulation. Z Metallk. 2003;94:682-6.
[43] Gottstein G. Physical Foundations of Materials Science: Springer-Verlag Berlin Heidelberg; 2004.
[44] Alvaro A, Akselsen OM, Ren X, Kane P-A. Fatigue Properties of a 420 MPa Structural Steel at Low Temperature. The 25th International Ocean and Polar Engineering Conference. Kona, Big Island, Hawaii, USA2015. p. 331-7.
[45] Koyama M, Akiyama E, Tsuzaki K, Raabe D. Hydrogen-assisted failure in a twinning-induced plasticity steel studied under in situ hydrogen charging by electron channeling contrast imaging. Acta Mater. 2013;61:4607-18.

[46] Habib K, Koyama M, Tsuchiyama T, Noguchi H. Fatigue crack non-propagation assisted by nitrogen-enhanced dislocation planarity in austenitic stainless steels. Int J Fatigue. 2017;104:158-70.
[47] Koyama M, Akiyama E, Lee Y-K, Raabe D, Tsuzaki K. Overview of hydrogen embrittlement in high-Mn steels. Int J Hydrog Energy. 2017;42:12706-23.
[48] Habib K, Koyama M, Tsuchiyama T, Noguchi H. Visualization of dislocations through electron channeling contrast imaging at fatigue crack tip, interacting with pre-existing dislocations. Materials Research Letters. 2017;6:61-6.
[49] Koyama M, Akiyama E, Sawaguchi T, Raabe D, Tsuzaki K. Hydrogen-induced cracking at grain and twin boundaries in an Fe-Mn-C austenitic steel. Scr Mater. 2012;66:459-62.
[50] Zaefferer S, Elhami NN. Theory and application of electron channelling contrast imaging under controlled diffraction conditions. Acta Mater. 2014;75:20-50.
[51] Ogawa Y, Birenis D, Matsunaga H, Takakuwa O, Yamabe J, Prytz O, et al. The role of intergranular fracture on hydrogen-assisted fatigue crack propagation in pure iron at a low stress intensity range. Mater Sci Eng A. 2018;733:316-28.
[52] Yu W, Esaklul K, Gerberich WW. Fatigue threshold studies in Fe, Fe-Si, and HSLA steel: Part II. thermally activated behavior of the effective stress intensity at threshold. Metall Trans A. 1984;15:889-900.
[53] Gerberich WW, Yu W, Esaklul K. Fatigue threshold studies in Fe, Fe-Si, and HSLA steel: Part I. Effect of strength and surface asperities on closure. Metall Trans A. 1984;15:875-88.
[54] Vehoff H, Neumann P, Rothe W. Quasibrittle fracture and cleavage initiation in Fe–2·6Si single crystals in different environments. Metal Science. 2013;15:469-70.
[55] Hajilou T, Deng Y, Kheradmand N, Barnoush A. Hydrogen enhanced cracking studies on Fe-3wt%Si single and bi-crystal microcantilevers. Philos Trans A Math Phys Eng Sci. 2017;375.
[56] Marrow TJ, Cotterill PJ, King JE. Temperature Effects on the Mechanism of Time Independent Hydrogen Assisted Fatigue Crack-Propagation in Steels. Acta Metall Mater. 1992;40:2059-68.
[57] Takahashi Y, Nishikawa H, Oda Y, Noguchi H. Microscopic characterization of hydrogen-induced quasi-brittle fatigue fracture in low-strength carbon steel. Mater Lett. 2010;64:2416-9.
[58] Nishikawa H-a, Oda Y, Takahashi Y, Noguchi H. Microscopic Observation of the Brittle-Striation Formation Mechanism in Low Carbon Steel Fatigued in Hydrogen Gas. J Solid Mech Mater Eng. 2011;5:179-90.
[59] Nishikawa H-a, Oda Y, Noguchi H. Investigation of the Mechanism for Brittle-Striation Formation in Low Carbon Steel Fatigued in Hydrogen Gas. J Solid Mech Mater Eng. 2011;5:370-85.
[60] Takahashi Y, Tanaka M, Higashida K, Yamaguchi K, Noguchi H. An intrinsic effect of hydrogen on cyclic slip deformation around a {110} fatigue crack in Fe–3.2wt.% Si alloy. Acta Mater. 2010;58:1972-81.
[61] Ogawa Y, Birenis D, Matsunaga H, Thogersen A, Prytz O, Takakuwa O, et al. Multi-scale observation of hydrogen-induced, localized plastic deformation in fatigue-crack propagation in a pure iron. Scr Mater. 2017;140:13-7.
[62] Ogawa Y, Matsunaga H, Yamabe J, Yoshikawa M, Matsuoka S. Unified evaluation of hydrogen-induced crack growth in fatigue tests and fracture toughness tests of a carbon steel. Int J Fatigue. 2017;103:223-33.
[63] Robertson IM, Sofronis P, Nagao A, Martin ML, Wang S, Gross DW, et al. Hydrogen Embrittlement Understood. Metall Mater Trans B. 2015;46:1085-103.
[64] Caillard D. A TEM in situ study of alloying effects in iron. II—Solid solution hardening caused by high concentrations of Si and Cr. Acta Mater. 2013;61:2808-27.
[65] Das A. Revisiting Stacking Fault Energy of Steels. Metall Mater Trans A. 2015;47:748-68.